Scientific Annals of Computer Science vol. 32 (2), 2022, pp. 255–283
doi: 10.7561/SACS.2022.2.255

An Enhanced Fluid Registration for Image Multi-Frame Super Resolution

Amine Laghrib[1], Aissam Hadri[2], Moad Hakim[3]

Abstract

The main idea of multi-frame super resolution (SR) algorithms is to recover a single high-resolution image from a sequence of low resolution ones of the same object. The success of the SR approaches is often related to a well registration and restoration steps. Therefore, we propose a new approach based on fluid image registration and we use a second order partial differential equation (PDE) to treat both the registration and restoration steps that guarantees the success of SR algorithms. Since the registration step is usually a variational ill-posed model, a mathematical study is needed to check the existence of the solution to the regularized problem. Thus, we prove the existence and uniqueness of the well posed fluid image registration and assure also the existence of the used second order PDE in the restoration step. The results show that the proposed method is competitive with the existing methods.

Keywords: Super resolution, Second order PDE, Fluid registration, Image restoration, Regularization.

[1]EMI FST Béni-Mellal, Université Sultan Moulay Slimane, Maroc, Email: laghrib.amine@gmail.com

[2]Université Ibn Zohr, Faculté polydisciplinaire, Ouarzazate, Maroc, Email: a.hadri@gmail.com

[3]EMI FST Béni-Mellal, Université Sultan Moulay Slimane, Maroc, Email: m.hakim@gmail.com

1 Introduction

Image super resolution represents an active research area in the imagery domain. The main principle of this method is to recover a high-resolution (HR) image through a single image (Single-image SR) [38, 35, 19], or using a series of low-resolution (LR) ones that are down-sampled, ill-registered, blurred and usually noised (multi-frame SR) [42, 24, 11]. SR intervenes in numerous domains, such as video surveillance and medical diagnostics [16].

The multi-frame and single SR are both intensively studied in order to improve the resolution of an image. In single SR technique, the missing information in the LR image is estimated from a large number of training. Then it success depends on the availability of a convenient dictionary which is not ensured in large application areas. While for the multi-frame SR the success is related to the approximation accuracy of the motion between the LR images. Since multiframe SR is more complicated in the presence of different degradation operators, Sina Farsiu et al [13] proposed the fast robust super resolution (RSR). The aim of this new technique is to break down the SR method into two steps: looking for a degraded HR image from the estimated LR frames after a registration procedure; then in a second step, restoring it [22].

On another side, the Euler-Lagrange equation associated to nonlinear PDEs have also been treated in the super-resolution context with great results. One of the consistent nonlinear PDE was proposed by Maiseli et al. [28], which takes the advantages of perona-Malik equation and the TV norm. This adaptive diffusion-based PDE can efficiently preserve image features but it suffers from the blurring effect. A more robust PDE was proposed by El Mourabit et al. [11] which take into consideration the coherence-enhancing property and avoids blur much better. However, when the blur and noise levels are too high, the obtained HR image still contain some artefacts, in particular the blur. More recently a fourth-order nonlinear PDE is then introduced with much more constrained diffusion that stops the edges destruction and preserve the smooth areas and texture [23]. In contrast, the blur apparition problem still a remaining weakness of this PDE.

The first step of multiframe SR aim is to guest the motion between the LR frames to register all LR images in a common way [44]. This stage is the key of the success of multiframe SR algorithms and without a good estimation of the motion between the LR sequence, the super-resolution becomes very limited [5].

Afterwards, the selection of a regularization function in the deblurring

and denoising process (the last step of SR technique) is very important to avoid different artefacts. Indeed, great care must be made in the choice of this function. There is numerous of super-resolution approaches that rely on regularization framework [17, 12, 29]. Even if these methods give promising results they have some shortcomings. One of them is the staircasing effect and the blur apparition in the flat regions. Although the noise and blur, in smooth regions, can be reduced by adjusting the regularization parameter, the texture information is however blurred.

Furthermore, deep learning has been widely used to address the single image super-resolution task. One of the famous work is the one proposed by Dong et al. [9], where the authors introduce the CNN-based SR method (SRCNN), which is done in three convolutional steps. The three steps are realized such as: patch extraction, non-linear mapping, and reconstruction. The SRCNN has shown attractive results, however, the need of large HR images for data training still an ambarrassing problem. Then, Dong et al. introduced an accelerated version of SRCNN which called FSRCNN [8], which aims is to incorporate the upsampling operation into the network. As a result, the restoration quality is efficient in a remarkable execution time. In contrast, this approach remains relatively shallow. Other approaches are then elaborated to fix the issues of the previous approach, see [18] for more details. Recently, Zhang et al. [43] used more advances on deep learning to propose the similar network (DnCNN), which shows great success. More recently, Chen et al.[6] investigated a deep convolutional network-based SR (CISRDCNN) framework for compressed images, which gives promising results.

In this paper, we follow the steps of the RSR method, while the registration approach and the second step are improved. In fact, we are developed two things:

- ⋆ We propose a modified fluid image registration in a well-posed functional framework independent of time to handle the registration part of the super-resolution part.

- ⋆ To ensure this choice, we show the existence and the uniqueness of the solution using classical mathematics approaches [1, 20].

- ⋆ Since the problems of deblurring and denoising are in most cases ill-posed, in the second step of SR, we introduce a fourth order PDE to remove noise and blur.

⋆ The two modified steps help to increase the robustness of the of the proposed SR algorithm. This is justified in the numerical part.

This paper follows this configuration: Section 2 introduces the super resolution formulation. We introduce then the fluid registration and how to define the deformations operators in Section 3. In Section 4, we describe briefly the proposed PDE and the main algorithm used in the deconvolution and denoising step. Finally, simulated and real results with comparisons of the proposed SR method to some available methods are presented in Section 5.

2 Problem Formulation

In the presence of many degradation factors, the acquired images are always in a non desired resolution. In fact, the obtained images are decimated, noised and also blurred. We consider that the LR images are taken in the same conditions with one sensor. The link between the HR image X (described by a vector of size $[r^2N^2 \times 1]$ where r is the enhancement factor) and the associated low resolution frames Y_k (represented by a vector of size $[N^2 \times 1]$), is given by

$$Y_k = DF_kHX + e_k \qquad \forall k = 1, 2, \ldots, n, \tag{1}$$

where:

H: the convolution operator describing the blur of size $[r^2N^2 \times r^2N^2]$.

D: the decimation operator which is related to the desired resolution of the HR image of size $[N^2 \times r^2N^2]$.

F_k: are the motions or the warp matrix of size $[r^2N^2 \times r^2N^2]$, representing randomize transformation between the LR frames.

e_k: is the additive Gaussian noise vector of size $[N^2 \times 1]$.

The aim of multi-frame super resolution is the recovery of an ideal HR image X. Due to the complexity of the problem we split it in two procedure [13]:

1. Approximating the transformation matrix F_k between each couple of LR images and merge the HR image B with noise and blur.
2. Computing the HR image X through the blurring and noisy one B.

We start by the approximation of the warp matrix F_k and also by ensuring the existence of the solution in a suitable functional space [30, 24, 3].

3 The Construction of the Warp Matrix F_k

We obtain the warp matrix F_k for each frame through a fluid registration algorithm, after a transition from discrete to continuous images using 2-linear interpolation. Let us denote by $Y_k(x)$ the intensity of the kth image at coordinate $x \in \Omega \subset \mathbb{R}^2$, where Ω is defined as the domain of the image. The image registration problem is formulated as

$$Y(x) = Y_k(v_k(x)) \qquad \text{for } k = 2, \ldots, n \quad \text{and} \quad \forall x \in \Omega. \tag{2}$$

Our goal is to find the velocity deformation v_k between the images, where

$$v_k = \partial_t u_k + \nabla u_k . v_k, \tag{3}$$

u_k are the deformations between each frame. Unfortunately, this problem is ill-posed. We have therefore to choose an appropriate regularization operator S. Since we know the success of the fluid registration to handle different problems in image registration [27], we propose to use it in a well-posed functional framework. The image fluid registration problem is defined as

$$\begin{cases} \min\limits_{u_k \in \mathcal{T}} \mathcal{J}(u_k), \text{where } \mathcal{J}(u_k) = \mathcal{D}(Y, Y_k, u_k) + \beta S(v_k), \\ \text{such that } v_k = u_k + \nabla u_k . v_k, \end{cases} \tag{4}$$

where $\mathcal{T}$ denotes the set of admissible transformations, and β the regularisation parameter.

$\mathcal{D}$: is the squared difference measure defined by Lebesgue L^2 norm as

$$\mathcal{D}(Y, Y_k, u_k) = \int_\Omega \left(Y_k(u_k(x)) - Y(x)\right)^2 dx, \tag{5}$$

and the fluid regularisation is defined as

$$S(v_k) = \int_\Omega \mu \left(\text{trace}V\right)^2 + \frac{\lambda}{2} \text{trace}(V^2) dx, \tag{6}$$

where V is the Cauchy strain tensor (for $||\nabla v_k|| \leq 1$) defined as $V(v_k) = (\nabla v_k + \nabla v_k^\intercal)/2$, and μ and λ are the Lamé parameters. To ensure the existence of a unique solution to the problem (4), we have to chose firstly a functional framework. A natural choice of the functional space is the Sobolev space $H_0^1(\Omega)$. To demonstrate the ellipticity of $\mathcal{J}$ and the strict

convexity, we use the Korn's inequality [31]. Thus, the admissible space of transformation is defined as

$$\mathcal{T} = H_0^1(\Omega). \tag{7}$$

We use also a classical result [2] to show the lower semi-continuity (l.s.c) of the function $\mathcal{J}$. In the following, we present the main theorem of the existence and uniqueness of the solution to the proposed fluid image registration.

Theorem 1 *Let Ω be a regular bounded open subset of $\mathbb{R}^2$, and let f be in $L^2(\Omega)$. Then, the minimization problem*

$$\min_{u_k \in \mathcal{T}} \mathcal{J}(u_k), \tag{8}$$

admits a unique solution.

Proof: To demonstrate that the function $\mathcal{J}$ admits a unique solution, we use the classical steps in optimization [10], i.e. we prove that $\mathcal{J}$ is elliptic and weakly sequentially l.s.c. We start by the ellipticity.

ellipticity: Using the propriety of the strain tensor in (6), we can reformulate it as

$$S(v_k) = \int_\Omega \frac{\mu}{4} \sum_{j,i=1}^{2} (\partial x_j v_{k_i} + \partial x_i v_{k_j})^2 + \frac{\lambda}{2}(div(v_k))^2 dx. \tag{9}$$

We need also to define the semi-norm

$$|\varepsilon(v_k)|_0 = \left(\int_\Omega \text{trace}(V(v_k)^T . V(v_k)) \right)^{1/2}.$$

Let $u_k \in \mathcal{T}$. Then

$$\begin{aligned}
\mathcal{J}(u_k) &= \int_\Omega \mu \, trace(V(v_k)^\top V(v_k)) + \frac{\lambda}{2} \, trace(V(v_k))^2 \, dx \\
&\quad + \int_\Omega (Y_k(u_k(x)) - Y(x))^2 \, dx \\
&\geq \mu \int_\Omega trace(V(v_k)^\top V(v_k)) dx + \int_\Omega (Y_k(u_k(x)) - Y(x))^2 \, dx \\
&\geq \mu |\varepsilon(v_k)|_0^2 - \|f\|_{L^2(\Omega)} \|u_k\|_{H^1(\Omega)},
\end{aligned} \tag{10}$$

where $\|f\|_{L^2(\Omega)} = \|Y\|_{L^\infty(\Omega)} \times \|Y_k\|_{L^2(\Omega)}$. Using the Korn's inequality, we can deduce that it exist a constant $\beta > 0$ such that

$$\|u_k\|_{H^1(\Omega)} \leq \beta |\varepsilon(v_k)|_0. \tag{11}$$

By setting $C = \frac{\mu}{\beta}$ this implies that

$$\mathcal{J}(u_k) \geq C\|u_k\|^2_{H^1(\Omega)} - \|f\|_{L^2(\Omega)}\|u_k\|_{H^1(\Omega)}. \tag{12}$$

Using the Young inequality, we have

$$\begin{aligned}\mathcal{J}(u_k) &\geq C\|u_k\|^2_{H^1(\Omega)} - C(\epsilon)\|f\|^2_{L^2(\Omega)} - \frac{\epsilon}{2}\|u_k\|^2_{H^1(\Omega)} \\ &\geq (C - \frac{\epsilon}{2})\|u_k\|^2_{H^1(\Omega)} - C(\epsilon)\|f\|^2_{L^2(\Omega)},\end{aligned} \tag{13}$$

where the parameter ε is chosen such as $C - \frac{\varepsilon}{2} > 0$.

Finally, we can easily check that $\mathcal{J}(u_k) \to \infty$ if $\|u_k\|_{H^1(\Omega)} \to \infty$. This implies that $\mathcal{J}$ is elliptic.

Weak sequentially l.s.c.: To demonstrate the weak sequentially l.s.c, we have to prove that $\mathcal{J}$ is continuous and convex.

Continuity :

Let $(u_n)_{n\geq 0}$ be a sequence in $\mathcal{T}$ that converge to u, such as

$$\begin{cases} u_n \to u \ \ in\ L^2(\Omega), \\ and \\ \nabla u_n \to \nabla u \ \ in\ L^2(\Omega). \end{cases} \tag{14}$$

Then there exist a subsequence $(u_{n'})_{n'\geq 0}$ and a function $u \in L^2(\Omega)$ such as

$$u_{n'}(x) \to u(x)\ and\ |u_{n'}(x)| \leq v_1(x)\ a.e\ x \in \Omega, \tag{15}$$

and

$$\nabla u_{n'}(x) \to \nabla u(x)\ et\ |\nabla u_{n'}(x)| \leq v_2(x)\ for\ a.e\ \ x \in \Omega. \tag{16}$$

We get

$$V(u_{n'}(x)) = \frac{1}{2}(\nabla u_{n'}(x)^\top + \nabla u_{n'}(x)) \to V(u(x)) \qquad a.e\ x \in \Omega. \tag{17}$$

In addition their exist $h \in L^1(\Omega)$, such as

$$\left| \begin{array}{l} \mu \; trace(V(u_{n'}(x))^\top V(u_{n'}(x))) + \\ \dfrac{\lambda}{2} \; trace(V(u_{n'}(x)))^2 \; + \langle f, u_{n'}(x) \rangle \end{array} \right| \leq h(x). \tag{18}$$

Using the Lebesgue theorem, we have

$$J(u_{n'}) \to \mathcal{J}(u). \tag{19}$$

Strict convexity: We use a classical result of convexity based on the second derivative of $\mathcal{J}$. Let $u_k, w_k \in \mathcal{T}$, we have then

$$\begin{aligned} \mathcal{J}^{''}(u_k)(w_k - u_k, w_k - u_k) &= \int_\Omega \mu \; trace(V(w_k - u_k)^\top V(w_k - u_k)) \\ &\quad + \frac{\lambda}{2} \; trace(V(w_k - u_k))^2 \; dx \\ &\geq \int_\Omega \mu \; trace(V(w_k - u_k)^\top V(w_k - u_k)) dx. \end{aligned} \tag{20}$$

Using Korn's inequality, we have

$$\begin{aligned} J^{''}(u_k)(w_k - u_k, w_k - u_k) &\geq C \|w_k - u_k\|^2_{H^1(\Omega)} \\ &> 0 \quad \text{for } u_k \neq w_k \end{aligned} \tag{21}$$

This, shows the strict convexity of $\mathcal{J}$, and concludes the proof.

□

To solve the minimisation problem (8), we use the BFGS algorithm [34]. We finally find the warp matrix F_k using $\hat{u}_k$ (the solution of the problem (8)). For the fusion step, we use the algorithm in [25, 39] to compute the blurred and noisy HR image $B = HX$. After that, we carry out the last step of the SR algorithm, which is the restoration step.

4 Restoration Step

Since the problem of restoration is ill-posed, we have to be careful in the choice of a suitable approach for denoising and deconvolution step. The main purpose of this stage is to preserve image features and avoid the blocky effect while reducing noise and blur using high-order operator [40]. A robust

higher-order total variation model is proposed as an efficient solution to the blocky effect, called total generalised variation (TGV) [37]. Even if this method avoids the staircasing effect, the computational time to reach the solution is very significant. An alternative way is to use a combined approach of the first and second order regularizer proposed by Papafitsoros et al. [32] which eliminate noise and blur avoiding the blocky artifacts in the HR in less time than the TGV. Let us describe briefly the algorithm used in the proposed SR approach. In this paper, we use the gradient descent PDE with a Neumann boundary condition on $\partial\Omega$, associated to the variational model proposed in [32]. This PDE with the initial condition $X(0,x) = X_0$ (where X_0 is the obtained HR image calculated by the interpolation of the LR image Y_1) is given by

$$\begin{cases} \partial_t X & = H^\intercal \operatorname{sign}(HX - B) + \gamma \operatorname{div}\left(\frac{g_1'(|\nabla X|)}{|\nabla X|}\nabla X\right) \\ & \quad +(1-\gamma)\operatorname{div}^2\left(\frac{g_2'(\|\nabla^2 X\|)}{\|\nabla^2 X\|}\nabla^2 X\right), \\ \partial_n X & = 0, \text{ on } \partial\Omega, \end{cases} \tag{22}$$

where the divergence operator $\operatorname{div} : (\mathbb{R}^{r^2N^2\times 1})^2 \longrightarrow \mathbb{R}^{r^2N^2\times 1}$, defined as

$$\operatorname{div} X.Y = X.\nabla Y,\ \forall X \in (\mathbb{R}^{r^2N^2\times 1})^2,\ Y \in \mathbb{R}^{r^2N^2\times 1}. \tag{23}$$

Also, the second-order divergence operator $\operatorname{div}^2 : (\mathbb{R}^{r^2N^2\times 1})^4 \longrightarrow \mathbb{R}^{r^2N^2\times 1}$, with the adjointness property, is defined

$$\operatorname{div}^2 X.Y = X.\nabla^2 Y,\ \forall X \in (\mathbb{R}^{r^2N^2\times 1})^4,\ Y \in \mathbb{R}^{r^2N^2\times 1}, \tag{24}$$

g_1 and g_2 are linear growth increasing functions defined: $\mathbb{R} \longrightarrow \mathbb{R}^+$ such as their exist four constants C_1, C_2, C_3, C_4 verifying

$$\begin{aligned} g_1(x) &\le C_1(1+|x|), \quad \forall x \in \mathbb{R} \\ g_2(x) &\le C_2(1+|x|), \quad \forall x \in \mathbb{R}. \end{aligned}$$

Also, we assume that both g_1 and g_2 are coercive:

$$\begin{aligned} g_1(x) &\ge C_3|x|, \quad \forall x \in \mathbb{R} \\ g_2(x) &\ge C_4|x|, \quad \forall x \in \mathbb{R}, \end{aligned}$$

and γ: the controlled regularization parameters. With this choice, we can reduce the staircasing compared to some previous SR methods. See for

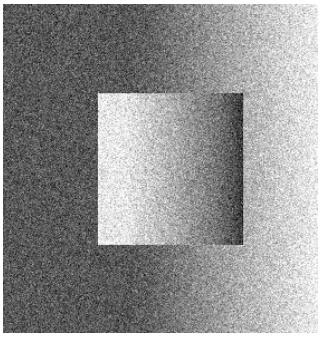

(a) Noisy image

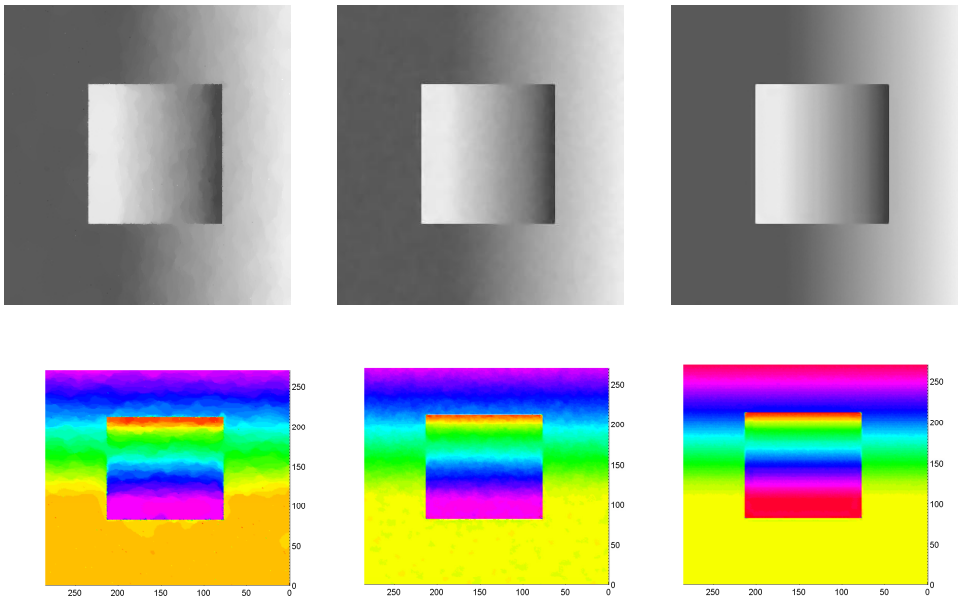

(b) HMR [15] (c) Our PDE (d) Original image

Figure 1: The efficiency of the fourth-order PDE in reducing the staircasing effect for the *Square* image, where the noise is considered to be a Gaussian one with standard deviation of $\sigma = 25$.

example Fig. 1, where we denoise the *square* image using the proposed approach and compared to the Huber-Markov regularization (HMR) [15].

The existence and uniqueness of solution to this PDE is demonstrated using the relaxation techniques [21], based on the monotony of the operators

$\operatorname{div}\left(\frac{g_1'(|\nabla X|)}{|\nabla X|}\nabla X\right)$ and $\operatorname{div}^2\left(\frac{g_2'(\|\nabla^2 X\|)}{\|\nabla^2 X\|}\nabla^2 X\right)$. To solve the PDE above, we use a classical finite difference scheme.

Let $X_{i,j}$ the discrete version of the image X, such as $X_{i,j} = X(i,j)$, $i = 1 \dots M$, $j = 1 \dots M$, where $M = rN$. We give briefly the discrete version of the operators ∇ and div given by

$$(\nabla X)^1_{i,j} = \begin{cases} X_{i+1,j} - X_{i,j} & \text{if} \quad i < M \\ 0 & \text{if} \quad i = M \end{cases}, \tag{25}$$

$$(\nabla X)^2_{i,j} = \begin{cases} X_{i,j+1} - X_{i,j} & \text{if} \quad j < M \\ 0 & \text{if} \quad j = M \end{cases}, \tag{26}$$

and

$$(\operatorname{div}(p^1, p^2))_{i,j} = (\operatorname{div}(p^1, p^2))^1_{i,j} + (\operatorname{div}(p^1, p^2))^2_{i,j}, \tag{27}$$

where

$$(\operatorname{div}(p^1, p^2))^1_{i,j} = \begin{cases} p^1_{i,j} - p^1_{i-1,j} & \text{if} \quad 1 < i < M \\ p^1_{i,j} & \text{if} \quad i = 1 \\ 0 & \text{if} \quad i = M \end{cases}, \tag{28}$$

$$(\operatorname{div}(p^1, p^2))^2_{i,j} = \begin{cases} p^2_{i,j} - p^2_{i,j-1} & \text{if} \quad 1 < j < M \\ p^2_{i,j} & \text{if} \quad j = 1 \\ -p^2_{i,j-1} & \text{if} \quad j = M \end{cases}. \tag{29}$$

Let us define the second order discrete differential operators noted ∇^2 as

$$\nabla^2 X = \begin{pmatrix} \nabla_{xx} X & \nabla_{xy} X & \nabla_{xy} X & \nabla_{yy} X \end{pmatrix}, \tag{30}$$

where

$$\nabla_{xx} X_{i,j} = \begin{cases} X_{i,M} - 2X_{i,1} + X_{i,2} & \text{if } 1 \le i \le M,\ j = 1, \\ X_{i,j-1} - 2X_{i,j} + X_{i,j+1} & \text{if } 1 \le i \le M,\ 1 < j < M, \\ X_{i,M-1} - 2X_{i,M} + X_{i,1} & \text{if } 1 \le i \le M,\ j = M, \end{cases} \tag{31}$$

$$\nabla_{yy} X_{i,j} = \begin{cases} X_{M,j} - 2X_{1,j} + X_{2,j} & \text{if } i = 1,\ 1 \le j \le M, \\ X_{i-1,j} - 2X_{i,j} + X_{i+1,j} & \text{if } 1 < i < M,\ 1 \le j \le M, \\ X_{M-1,j} - 2X_{M,j} + X_{1,i} & \text{if } i = M,\ 1 \le j \le M, \end{cases} \tag{32}$$

and

$$\nabla_{xy} X_{i,j} = \begin{cases} X_{i,j} - X_{i+1,j} - X_{i,j+1} + X_{i+1,j+1} & \text{if } 1 \leq i < M,\ 1 \leq j < M, \\ X_{i,M} - X_{i+1,M} - X_{i,1} + X_{i+1,1} & \text{if } 1 \leq i < M,\ j = M, \\ X_{M,j} - X_{1,j} - X_{M,j+1} + X_{1,j+1} & \text{if } i = M,\ 1 \leq j < M, \\ X_{M,M} - X_{1,M} - X_{M,1} + X_{1,1} & \text{if } i = M,\ j = M. \end{cases} \tag{33}$$

In addition, for $X = (X_1,\, X_2,\, X_3,\, X_4) \in \left(\mathbb{R}^M\right)^4$, we define the discrete div^2 operator as

$$(\mathrm{div}^2\, X)_{i,j} = \overline{\nabla_{xx}} X_{1_{i,j}} + \overline{\nabla_{yy}} X_{2_{i,j}} + \overline{\nabla_{xy}} X_{3_{i,j}} + \overline{\nabla_{xy}} X_{4_{i,j}}, \tag{34}$$

where

$$\overline{\nabla_{xx}} = \nabla_{xx},\ \overline{\nabla_{yy}} = \nabla_{yy}, \tag{35}$$

and

$$\overline{\nabla_{xy}} X_{i,j} = \begin{cases} X_{1,1} - X_{1,M_2} - X_{M_1,1} + X_{M_1,M_2} & \text{if } i = 1,\ j = 1, \\ X_{1,j} - X_{1,j-1} - X_{M_1,j} + X_{M_1,j-1} & \text{if } i = 1,\ 1 < j \leq M, \\ X_{i,1} - X_{i-1,M_2} - X_{i-1,1} + X_{i-1,M_2} & \text{if } 1 < i \leq M,\ j = 1, \\ X_{i,j} - X_{i,j-1} - X_{i-1,j} + X_{i-1,j-1} & \text{if } 1 < i \leq M,\ 1 < j \leq M. \end{cases} \tag{36}$$

To give a comprehensive form of this problem, we set the particular case where $g_1(x) = g_2(x) = x$. As a result, the algorithm related to solve numerically the proposed PDE is finally given in **Algorithm 1**.

5 Numerical Experiments

In this part, our aim is to we test the ability of the elaborated algorithm in the SR context. Many simulated and also real results were used to test the performance of the proposed SR method. The first part is dedicated to the evaluation of the registration part while the second and third parts concern the main proposed SR approach. To increase the ability of the proposed equation to better detect edges, we choose the so-called hypersurface minimal function [4] defined for both the functions g_1 and g_2 by

$$g_1(x) = g_2(x) = \sqrt{1 + x^2}. \tag{37}$$

The input HR image X^0 is build by a bicubic interpolation of the LR reference image Y_1. In the simulated experiments, we choose five examples

Algorithm 1 The proposed algorithm

Inputs: The blurred image B; the steepest descent parameter dt. the regularization parameter γ.

To avoid the derivative singularity when X is locally constant (in the special case where the denominator is equal to zero);

The procedure:

$$\widehat{X}_{i,j}^{n+1}=\widehat{X}_{i,j}^{n}+dt\big(H_{i,j}^{\intercal}\mathrm{sing}((H\widehat{X})_{i,j}^{n}-B_{i,j})\big)+dt\gamma\ \mathrm{div}_{i,j}^{1}\left(\frac{(\nabla\widehat{X})_{i,j}^{1}}{\sqrt{((\nabla\widehat{X})_{i,j}^{1})^2+((\nabla\widehat{X})_{i,j}^{2})^2+1}}\right)$$
$$+dt\gamma\ \mathrm{div}_{i,j}^{2}\left(\frac{(\nabla\widehat{X})_{i,j}^{2}}{\sqrt{((\nabla\widehat{X})_{i,j}^{1})^2+((\nabla\widehat{X})_{i,j}^{2})^2+1}}\right)$$
$$+dt\,(1-\gamma)\,\overline{\nabla_{xx}}\left(\frac{\nabla_{xx}\widehat{X}_{i,j}^{n}}{\sqrt{1+(\nabla_{xx}\widehat{X}_{i,j}^{n})^2+(\nabla_{yy}\widehat{X}_{i,j}^{n})^2+2(\nabla_{xy}\widehat{X}_{i,j}^{n})^2}}\right)$$
$$+dt\,(1-\gamma)\,\overline{\nabla_{yy}}\left(\frac{\nabla_{yy}\widehat{X}_{i,j}^{n}}{\sqrt{1+(\nabla_{xx}\widehat{X}_{i,j}^{n})^2+(\nabla_{yy}\widehat{X}_{i,j}^{n})^2+2(\nabla_{xy}\widehat{X}_{i,j}^{n})^2}}\right)$$
$$+2\,dt\,(1-\gamma)\,\overline{\nabla_{xy}}\left(\frac{\nabla_{xy}\widehat{X}_{i,j}^{n}}{\sqrt{1+(\nabla_{xx}\widehat{X}_{i,j}^{n})^2+(\nabla_{yy}\widehat{X}_{i,j}^{n})^2+2(\nabla_{xy}\widehat{X}_{i,j}^{n})^2}}\right)\quad i,j=1,\ldots,M$$

Output: The restored HR image $\widehat{X}$

in Fig.2, with different size and texture, to illustrate the performance of the proposed SR method. The used images are selected from the Berkeley database[4], which includes 300 images with various sizes (217×181, 256×256, 512×512 and 1024×1024) and colors.

To construct the simulated images, we follow the degradation model (1). The HR image was first shifted with sub-pixel displacements to produce N images, then, the sequence was convoluted with a PSF and finally, zero-mean Gaussian noise was added to each frame of the sequence. Concerning the convergence of the proposed algorithm, we end the execution at the first iteration n with respect to the error $\dfrac{\|\widehat{X}^{n+1}-\widehat{X}^{n}\|_1}{\|\widehat{X}^{n}\|_1}<10^{-5}$. To evaluate the performance of the proposed algorithm, the peak-signal-to-noise ratio (PSNR) and the structural similarity (SSIM) criterion are used. The PSNR is used to measure the quality of the estimated HR image, while the SSIM

[4] https://www2.eecs.berkeley.edu/Research/Projects/CS/vision/bsds/BSDS300/html/dataset/images.html

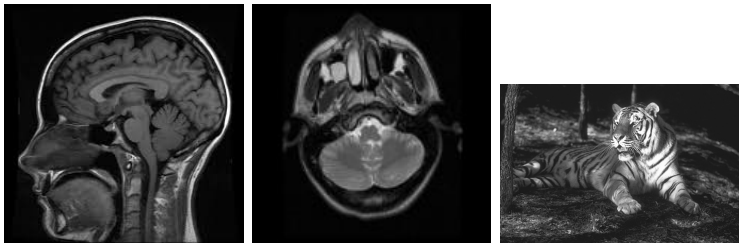

(a) MRI Brain 1 (b) MRI Brain 2 (c) Tiger

(d) Bird (e) Flowers

Figure 2: The original five images used in simulated tests

is a complementary measure, which gives an indication of image quality based on known characteristics of the human visual system. The PSNR is defined by

$$PSNR = 10 \log_{10} \left(\frac{255^2}{MSE} \right),$$

where the MSE is the mean squared error defined as

$$MSE = \frac{1}{MN} \Sigma_{i=1}^{M} \Sigma_{j=1}^{N} (Y(i,j) - X(i,j))^2.$$

The $SSIM$ is calculated on multiple windows of given image, i.e. the measurement between two windows x and y of size $N \times N$ is defined by

$$SSIM(x,y) = \frac{(2\mu_x\mu_y + c_1)(2\sigma_x\sigma_y + c_2)(2\, cov_{xy} + c_3)}{(\mu_x^2 + \mu_y^2 + c_1)(\sigma_x^2 + \sigma_y^2 + c_2)(\sigma_x\sigma_y + c_3)},$$

where the variables, respectively, defined for x and y as follows: μ_x and μ_y, mean; σ_x^2 and σ_y^2, variance; cov_{xy}, covariance; $c_1 = (m_1 L)^2$, $c_2 = (m_2 L)^2$ are two stabilizing constants; and L the dynamics of the pixel values, 255 for 8-bit encoded image.

5.1 The Effectiveness of the Registration Part

In the first experience, we construct 32 synthetic LR image from the original image of *MRI Brain 1* such as: each frame is deformed by random vector fields, blurred by a Gaussian low-pass filter with size 3×3 and a standard deviation of 1.5. Then, the blurred frames are down-sampled in the two directions by a factor of $r = 2$ and a Gaussian noise was added with a standard deviation $\sigma = 25$. In this test, we fix the deconvolution and denoising part where we use the proposed combined first and second order regularizer. Then, we compare our registration algorithm with other competitive registration methods in the SR context, such as: SR with probabilistic optical flow (POF) [14], SR with hyper-elastic (SRHE) [26], SR with deep neural network (Deepsum) [44], combining demons Registration (CDR) [7] and also SR with diffusion registration (SRDR) proposed in [25]. The obtained SR results are shown in Fig. 3 to see the efficiency of the proposed registration part. We can deduce that the proposed registration method gives a slightly better result compared to the other methods. For the second experiment, we consider the *MRI Brain 1* following the same previous steps with more complicated random deformations between the LR images. We increase also the decimation factor $r = 4$ and also the standard deviation $\sigma = 35$. The obtained HR image is depicted in Fig. 4, where comparison to other SR methods is done. Clearly the obtained HR image outperforms the other ones and the registration process is better enhanced.

To confirm the visual comparison, we use a qualitative illustration through the Signal-to-noise ratio (SNR) measure defined by:

$$SNR = \frac{EMM}{EML}$$
$$EML = \sum_{i=1}^{N}\sum_{j=1}^{M} X_{ij}^2$$
$$EML = \sqrt{\sum_{i=1}^{N}\sum_{j=1}^{M} (Y_{ij} - X_{ij})^2}$$

where Y is the clean image and X is the registered one using the denoising process. In fact, we present the obtained SNR values for the previous tests in Table 1 to show the efficiency of the proposed method in the super-resolution context. As expected, the proposed approaches outperforms the others in terms of SNR values, which validate the visual comparison.

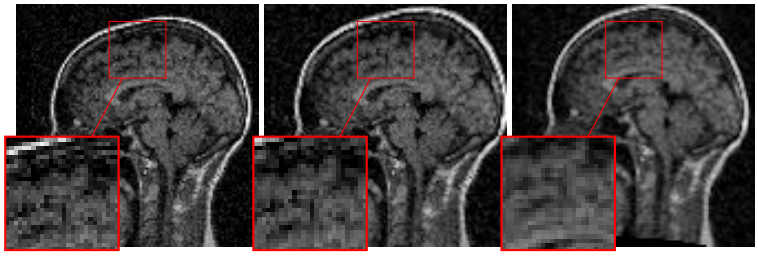

(a) First LR image (b) 16 th LR image (c) 18 th LR image

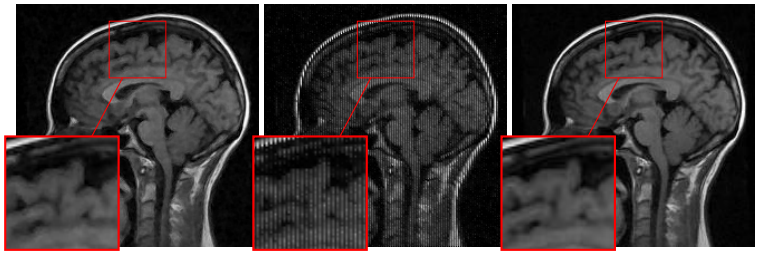

(d) CDR [7] (e) POF [14] (f) Deepsum [44]

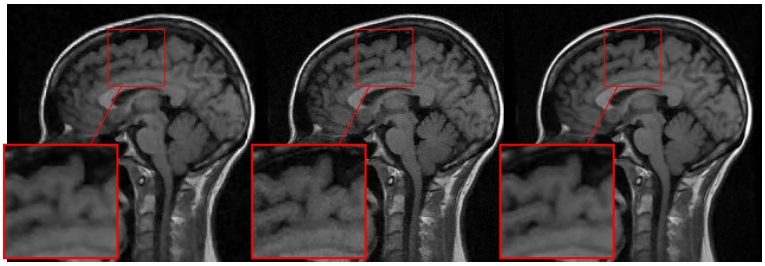

(g) SRHE [26] (h) SRDR [25] (i) Our method

Figure 3: Comparisons of different SR methods with different registration procedure of the (*MRI brain 1* image when the magnification factor is $r = 2$ using random motion vectors) to perform the registration step. Note that the noise is considered with a standard deviation $\sigma = 25$

Table 1: The SNR table of the two previous tests

Image	SNR values					
	POF [14]	SRHE [26]	CDR [7]	SRDR [25]	Deepsum [44]	Proposed approach
MRI Brain 1 ($r = 2$)	24.3333	26.0711	24.2222	28.3555	31.4766	**37.1466**
MRI Brain 1 ($r = 4$)	22.6648	24.7688	23.1737	25.2222	32.1133	**34.4399**
MRI Brain 2 ($r = 2$)	23.5555	24.6316	25.3493	28.2274	30.9333	**36.3644**
MRI Brain 2 ($r = 4$)	22.5245	24.0788	24.1111	27.3373	29.2886	**35.6895**

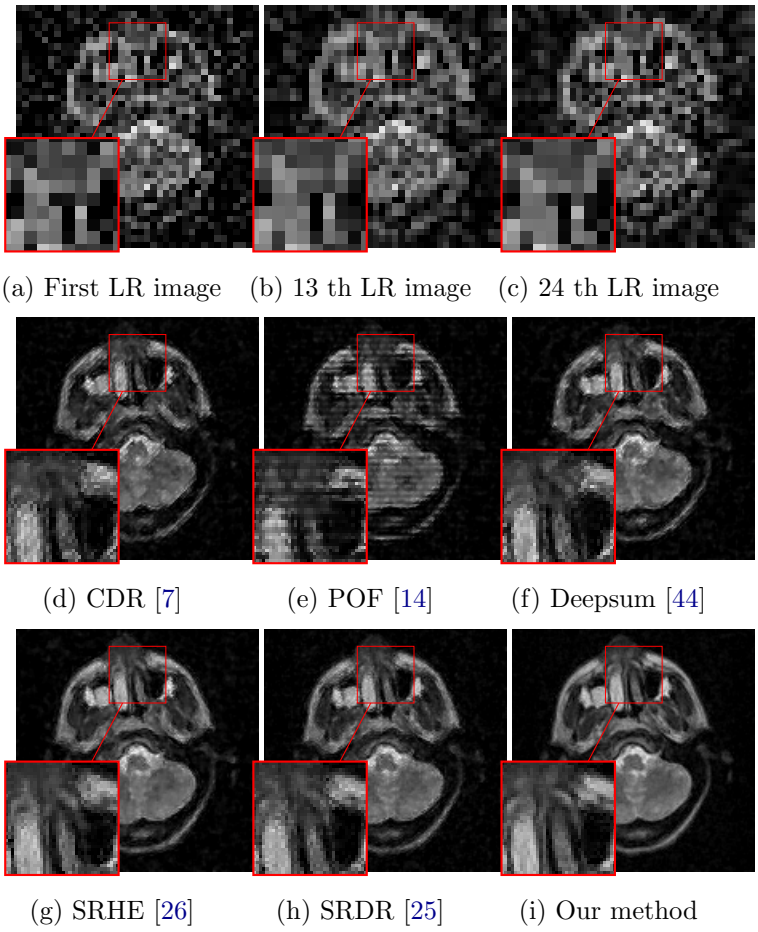

(a) First LR image (b) 13 th LR image (c) 24 th LR image

(d) CDR [7] (e) POF [14] (f) Deepsum [44]

(g) SRHE [26] (h) SRDR [25] (i) Our method

Figure 4: Comparisons of different SR methods with different registration procedure of the (*MRI brain 2* image when the magnification factor is $r = 4$ using random motion vectors) to perform the registration step. Note that the noise is considered with a standard deviation $\sigma = 35$.

5.2 The Effectiveness of the Second Order Regularization Term

To perform the restoration step of the proposed super-resolution approach, we fix now the registration step, which is considered as a fluid registration one for our method and also for the other SR approaches. We measure the performance of the proposed second order regularization term by considering a high-level of Gaussian noise, while the blur is supposed to be a Gaussian low-

pass filter with a size 3×3 and a standard deviation of 1.5. Indeed, we consider the LR frames from the *Tiger* original image corrupted by a Gaussian noise with $\sigma = 30$ respectively. The obtained results, when the magnification factor is $r = 4$, using different regularization terms, such as: nonlinear fourth-order PDE (FPDE) [23], nonlocal-means (NLM) [33], weighted TV (SWTV) [41], second-order combined model (SOM) [24] and bilateral spectrum weighted total variation (BSWTV) [36], are illustrated in the Fig. 5. Visually, we can see that the proposed second order regularization preserves the image features better than the other terms for the three noise level.

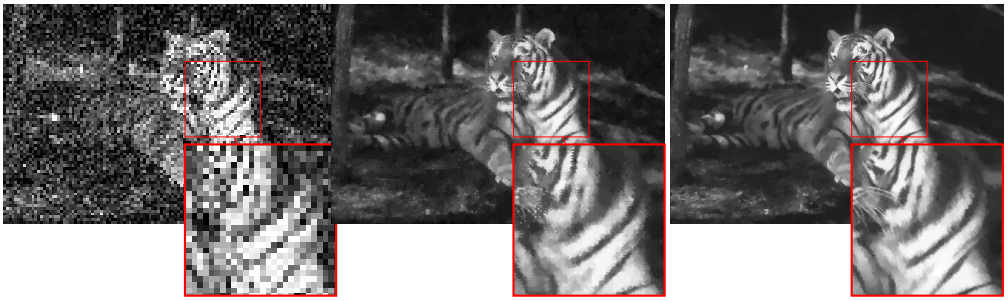

(a) One LR image (b) NLM [33] (c) SOM [24]

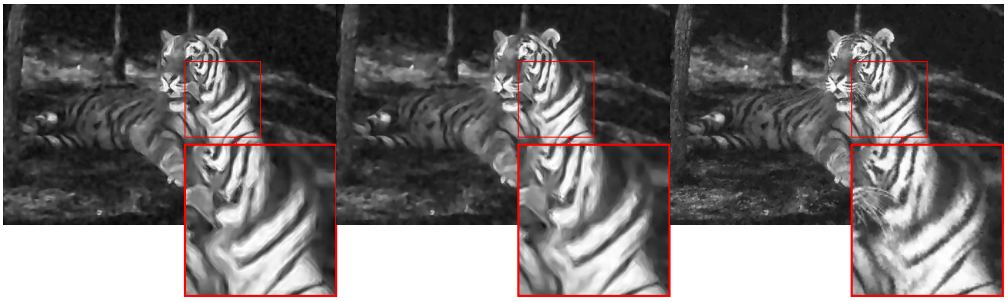

(d) *SWTV* method [41] (e) FPDE [23] (f) BSWTV [36]

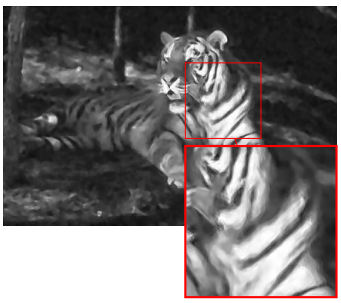

(g) The proposed SR

Figure 5: Super resolution of *the Tiger* compared with different methods.

In the second experiment, we keep the same procedure of the SR process except that this time the interest is to see how the proposed regularization term deals with high-level of blur and noise. Indeed, we consider the *Flowers* and we augment the blur level, which is considered now as a Gaussian low-pass filter with a size of 7×7 and a standard deviation of 2 while the noise is considered with $\sigma = 45$. Once again, as illustrated in the Fig. 6, the proposed regularization term outperforms the others in the quality of the restoration.

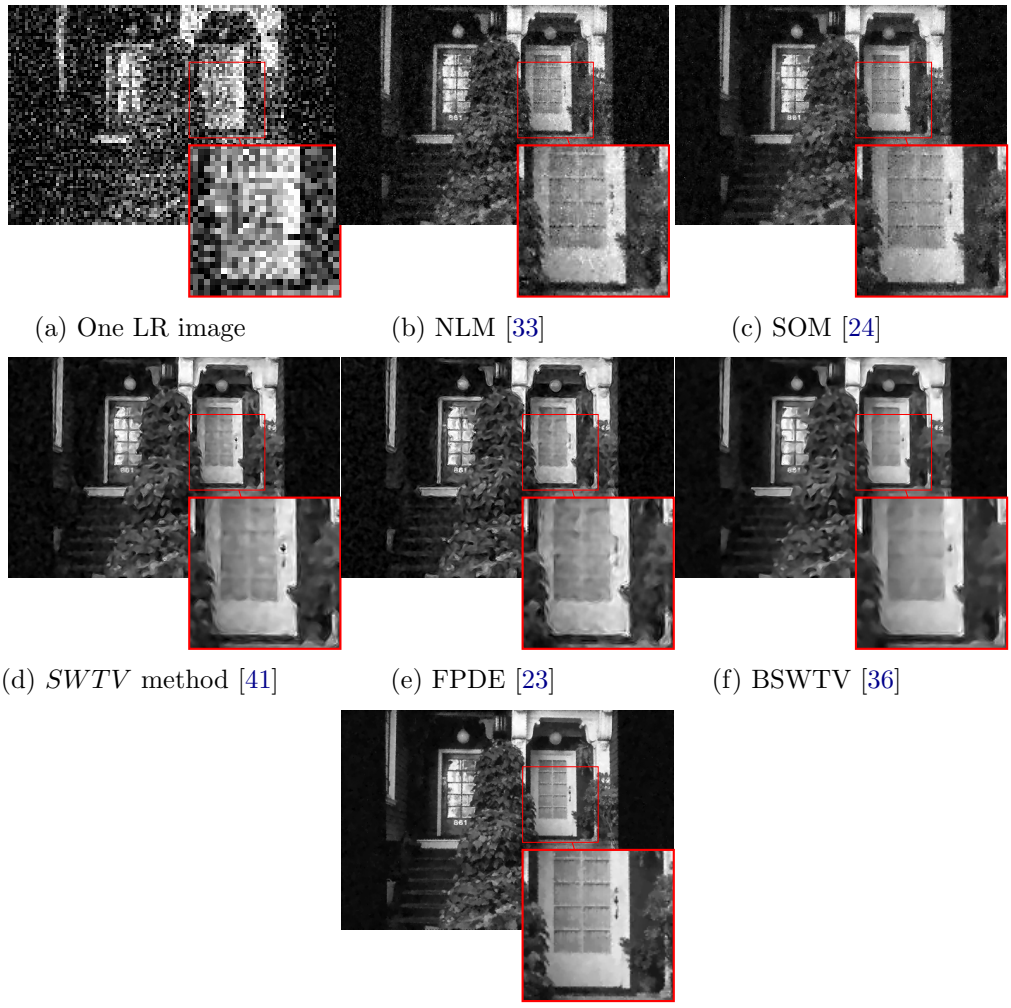

(a) One LR image (b) NLM [33] (c) SOM [24]

(d) *SWTV* method [41] (e) FPDE [23] (f) BSWTV [36]

(g) The proposed SR

Figure 6: Super resolution of *the Flowers* compared with different methods.

We use the same think for the third test of the *Bird* image, while we increase the blur kernel rate and σ noise for the other tests. Indeed, we use a 5×5 Gaussian blur kernel and a white Gaussian noise with $\sigma = 30$ to construct the sequence for the last four image. Concerning the choice of the parameters, the scalar weight γ is chosen according to the better PSNR value for the proposed and also for the other SR methods. For instance, we choose $\gamma = 0.55$ for *the Bird* image.

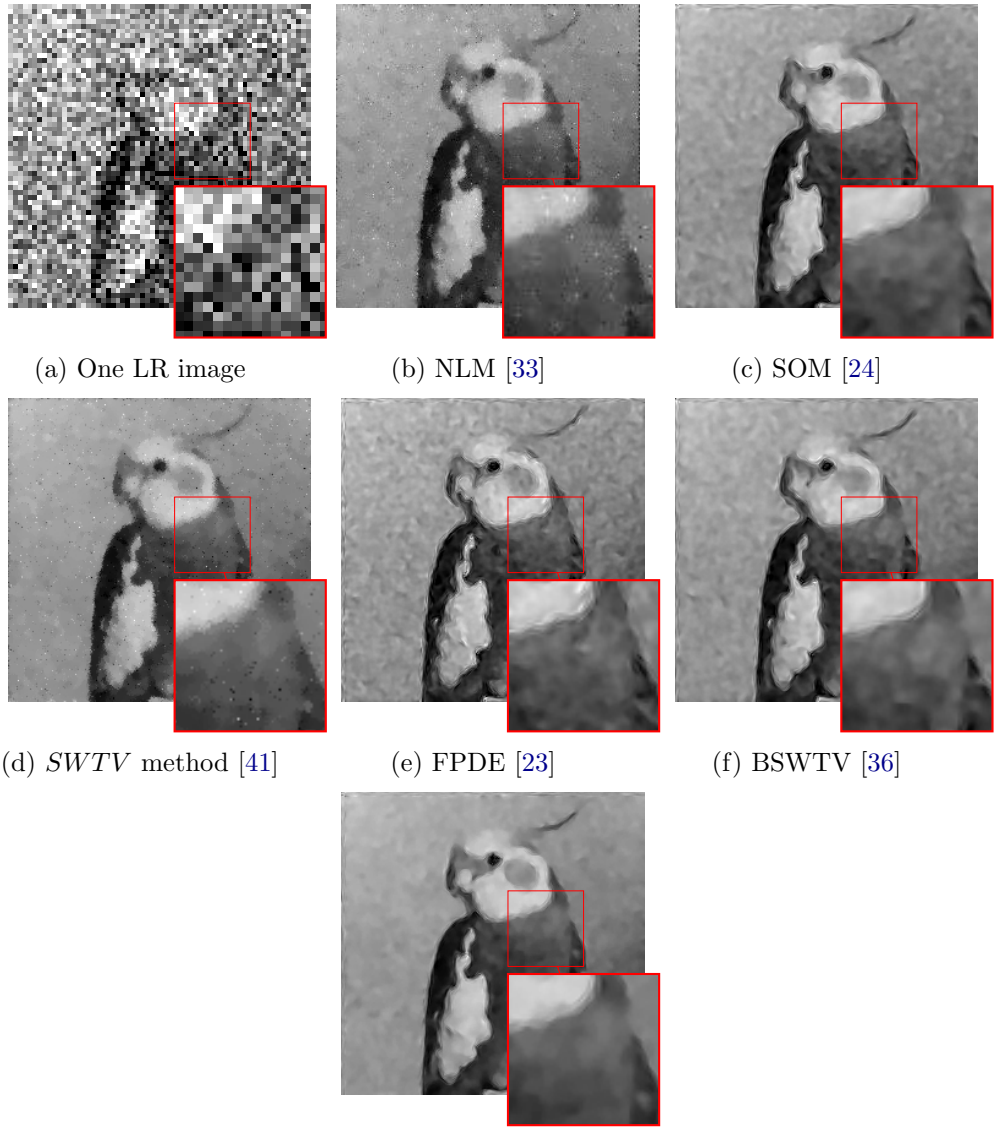

(a) One LR image (b) NLM [33] (c) SOM [24]

(d) *SWTV* method [41] (e) FPDE [23] (f) BSWTV [36]

(g) The proposed SR

Figure 7: Super resolution of the *Bird* compared with different methods.

To ensure the success of the proposed algorithm against noise and misregistration errors reducing, we use the PSNR criterion in the Table 2 and the SSIM measure in the Table 3 for the three previous tests. Knowing that the best score is in bold number, we can clearly show the efficiency of our algorithm. Also, visually, we can detect the performance of the proposed method in removing misregistration errors compared with the other methods in the smooth area, however, near strong edges, there is no distinct improvement compared to other methods.

Table 2: The PSNR table of the three previous tests. The bold number represents the high value in each line.

Image	PSNR values					
	POF [14]	SRHE [26]	CDR [7]	SRDR [25]	Deepsum [44]	Proposed approach
Tiger ($r = 2$)	28.88	28.22	28.17	28.66	29.26	**30.47**
Tiger ($r = 4$)	27.92	27.62	27.59	27.84	28.94	**29.89**
Flowers ($r = 2$)	28.18	28.07	28.58	28.97	30.06	**31.16**
Flowers ($r = 4$)	27.68	27.78	27.37	27.22	29.33	**30.29**
Bird ($r = 2$)	26.48	26.63	27.44	28.77	29.22	**30.06**
Bird ($r = 4$)	25.88	25.93	26.11	26.73	28.88	**29.66**

Table 3: The SSIM table of the three previous tests. The bold number represents the high value in each line.

Image	PSNR values					
	POF [14]	SRHE [26]	CDR [7]	SRDR [25]	Deepsum [44]	Proposed approach
Tiger ($r = 2$)	0.8277	0.8344	0.8527	0.8499	0.8609	**0.8814**
Tiger ($r = 4$)	0.8209	0.8184	.8376	0.8333	0.8517	**0.8729**
Flowers ($r = 2$)	0.8662	0.8533	.8699	0.8733	0.8794	**0.8937**
Flowers ($r = 4$)	0.8444	0.8527	0.8627	0.8652	0.8666	**0.8399**
Bird ($r = 2$)	0.8008	0.8102	0.8222	0.8288	0.8366	**0.8496**
Bird ($r = 4$)	.7866	0.7933	0.7949	0.7897	0.7992	**0.8109**

5.3 Real Experiments

In the real experiments, two real data sequences are used to approve the proposed algorithm are presented : the *Rocket* and *City* videos. We select the first twenty frames in the two real data sets. The diffusion registration approach presented in [25] is used as the registration estimation method for the other methods while we use the proposed fluid registration to estimate the motion for our method. The reconstruction results of these sequences are, respectively, shown in Figs. 8 and 9, where the magnification factor is

selected such as: $r = 2$ and $r = 4$. From these figures, it is shown that the proposed approach gives a better visual effect compared to the other method.

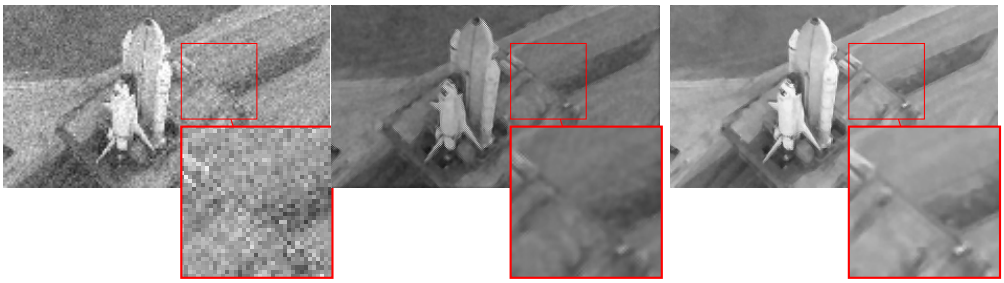

(a) One LR image (b) NLM [33] (c) SOM [24]

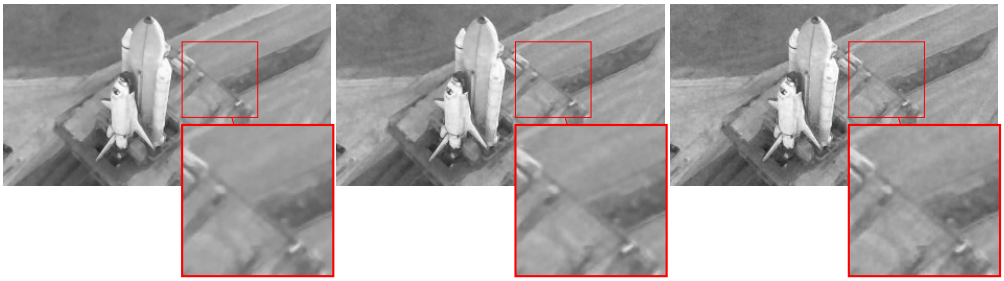

(d) *SWTV* method [41] (e) FPDE [23] (f) BSWTV [36]

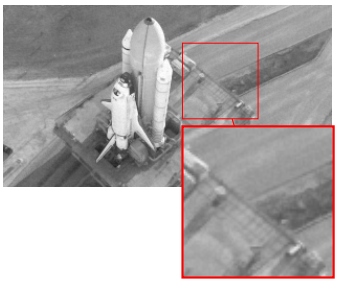

(g) The proposed SR

Figure 8: Results on the *Rocket* sequence.

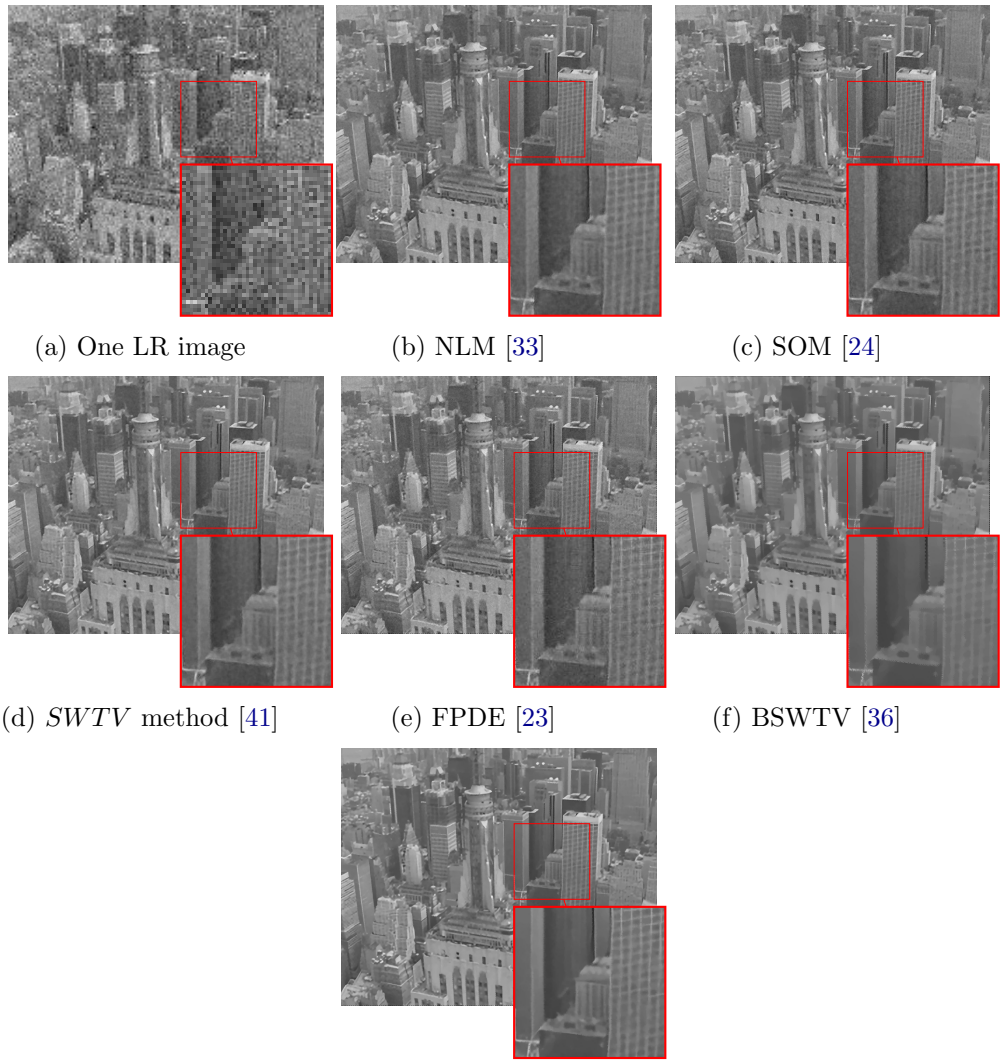

(a) One LR image (b) NLM [33] (c) SOM [24]

(d) *SWTV* method [41] (e) FPDE [23] (f) BSWTV [36]

(g) The proposed SR

Figure 9: Results on the *City* sequence.

6 Conclusion

In this paper, a novel approach of the super resolution image reconstruction problem is introduced. We presented a fluid image registration and proved the existence and uniqueness of the solution using the classical functional

analysis. In addition, to avoid the undesirable staircasing effect during the registration, denoising and deconvolution steps, a fourth order PDE is proposed. To confirm the robustness of this approach, a set of benchmark image have been performed, and the investigated SR approach has proven its success visually and also quantitatively using two known metrics. A remaining question is about the treatment of other types of noise and blur, such as Salt& paper and Poisson noise. As a future work, we will adopt some learning techniques about the choice of the parameter γ and also the regularization part to reduce the remaining blur in the restored images. Another interesting point is about the degrees of the efficiency of the proposed approach with respect to the nature of the transformations between the LR frames. As a future work, we will also adopt some learning techniques about the choice of the parameter γ and also the regularization part to reduce the remaining blur in the restored images.

Acknowledgements

We are very grateful to the anonymous reviewers for their insightful remarks and corrections.

Conflict of interest

The authors have no conflict of interest.

References

[1] Lekbir Afraites, Aissam Hadri, and Amine Laghrib. A denoising model adapted for impulse and Gaussian noises using a constrained-PDE. *Inverse Problems*, 36(2):025006, 2020. doi:10.1088/1361-6420/ab5178.

[2] Lekbir Afraites, Aissam Hadri, Amine Laghrib, and Mourad Nachaoui. A non-convex denoising model for impulse and Gaussian noise mixture removing using bi-level parameter identification. *Inverse Problems and Imaging*, 16(4):827–870, 2022. doi:10.3934/ipi.2022001.

[3] Mohamed Alahyane, Abdelilah Hakim, Amine Laghrib, and Said Raghay. A fast approach of nonparametric elastic image registration problem. *Mathematical Methods in the Applied Sciences*, 42(18):7059–7075, 2019. doi:10.1002/mma.5810.

[4] Gilles Aubert and Pierre Kornprobst. *Mathematical Problems in Image Processing - Partial Differential Equations and the Calculus of Variations, 2nd Edition*, volume 147 of *Applied Mathematical Sciences*. Springer, 2006.

[5] Simon Baker and Takeo Kanade. Limits on super-resolution and how to break them. *IEEE Transactions on Pattern Analysis and Machine Intelligence*, 24(9):1167–1183, 2002. doi:10.1109/TPAMI.2002.1033210.

[6] Honggang Chen, Xiaohai He, Chao Ren, Linbo Qing, and Qizhi Teng. CISRDCNN: super-resolution of compressed images using deep convolutional neural networks. *Neurocomputing*, 285:204–219, 2018. doi:10.1016/j.neucom.2018.01.043.

[7] Thaís Pedruzzi do Nascimento and Evandro Ottoni Teatini Salles. Multi-frame super-resolution combining demons registration and regularized Bayesian reconstruction. *IEEE Signal Processing Letters*, 27:2009–2013, 2020. doi:10.1109/LSP.2020.3033422.

[8] Chao Dong, Chen Change Loy, and Xiaoou Tang. Accelerating the super-resolution convolutional neural network. In Bastian Leibe, Jiri Matas, Nicu Sebe, and Max Welling, editors, *14th European Conference on Computer Vision, ECCV 2016*, volume 9906 of *Lecture Notes in Computer Science*, pages 391–407. Springer, 2016. doi:10.1007/978-3-319-46475-6_25.

[9] Weisheng Dong, Lei Zhang, Guangming Shi, and Xiaolin Wu. Image deblurring and super-resolution by adaptive sparse domain selection and adaptive regularization. *IEEE Transactions on Image Processing*, 20(7):1838–1857, 2011. doi:10.1109/TIP.2011.2108306.

[10] Abdelmajid El Hakoume, Lekbir Afraites, and Amine Laghrib. An improved coupled PDE system applied to the inverse image denoising problem. *Electronic Research Archive*, 30(7):2618–2642, 2022. doi:10.3934/era.2022134.

[11] Idriss El Mourabit, Mohammed El Rhabi, Abdelilah Hakim, Amine Laghrib, and Eric Moreau. A new denoising model for multi-frame super-resolution image reconstruction. *Signal Processing*, 132:51–65, 2017. doi:10.1016/j.sigpro.2016.09.014.

[12] Idriss El Mourabit, Abdelilah Hakim, and Amine Laghrib. An anisotropic PDE for multi-frame super-resolution image reconstruction. In Abdeljalil Nachaoui, Abdelilah Hakim, and Amine Laghrib, editors, *Mathematical Control and Numerical Applications*, pages 29–41. Springer International Publishing, 2021. doi:10.1007/978-3-030-83442-5_3.

[13] Sina Farsiu, M Dirk Robinson, Michael Elad, and Peyman Milanfar. Fast and robust multiframe super resolution. *IEEE Transactions on Image Processing*, 13(10):1327–1344, 2004. doi:10.1109/TIP.2004.834669.

[14] Rik Fransens, Christoph Strecha, and Luc Van Gool. Optical flow based super-resolution: A probabilistic approach. *Computer Vision and Image Understanding*, 106(1):106–115, 2007. doi:10.1016/j.cviu.2005.09.011.

[15] Debabrata Ghosh, Naima Kaabouch, and Wen-Chen Hu. A robust iterative super-resolution mosaicking algorithm using an adaptive and directional Huber-Markov regularization. *Journal of Visual Communication and Image Representation*, 40:98–110, 2016. doi:10.1016/j.jvcir.2016.06.008.

[16] Hayit Greenspan, G Oz, N Kiryati, and SLBG Peled. MRI inter-slice reconstruction using super-resolution. *Magnetic resonance imaging*, 20(5):437–446, 2002. doi:10.1016/s0730-725x(02)00511-8.

[17] Aissam Hadri, Hamza Khalfi, Amine Laghrib, and Mourad Nachaoui. An improved spatially controlled reaction–diffusion equation with a non-linear second order operator for image super-resolution. *Nonlinear Analysis: Real World Applications*, 62:103352, 2021. doi:10.1016/j.nonrwa.2021.103352.

[18] Khizar Hayat. Multimedia super-resolution via deep learning: A survey. *Digital Signal Processing*, 81:198–217, 2018. doi:10.1016/j.dsp.2018.07.005.

[19] Neeraj Kumar, Ruchika Verma, and Amit Sethi. Convolutional neural networks for wavelet domain super resolution. *Pattern Recognition Letters*, 90:65–71, 2017. doi:10.1016/j.patrec.2017.03.014.

[20] Amine Laghrib, Lekbir Afraites, Aissam Hadri, and Mourad Nachaoui. A non-convex PDE-constrained denoising model for impulse and Gaussian

noise mixture reduction. *Inverse Problems and Imaging*, 2022. doi:10.3934/ipi.2022031.

[21] Amine Laghrib, Fatimzehrae Aitbella, and Abdelilah Hakim. A second-order nonlocal regularized variational model for multiframe image super-resolution. *International Journal of Nonlinear Sciences and Numerical Simulation*, 23(3-4):385–399, 2021. doi:10.1515/ijnsns-2019-0109.

[22] Amine Laghrib, A Ben-Loghfyry, Aissam Hadri, and Abdelilah Hakim. A nonconvex fractional order variational model for multi-frame image super-resolution. *Signal Processing: Image Communication*, 67:1–11, 2018. doi:10.1016/j.image.2018.05.011.

[23] Amine Laghrib, Abdelkrim Chakib, Aissam Hadri, and Abdelilah Hakim. A nonlinear fourth-order PDE for multi-frame image super-resolution enhancement. *Discrete & Continuous Dynamical Systems-B*, 25(1):415–442, 2020. doi:10.3934/dcdsb.2019188.

[24] Amine Laghrib, Mahmoud Ezzaki, Mohammed El Rhabi, Abdelilah Hakim, Pascal Monasse, and Said Raghay. Simultaneous deconvolution and denoising using a second order variational approach applied to image super resolution. *Computer Vision and Image Understanding*, 168:50–63, 2018. doi:10.1016/j.cviu.2017.08.007.

[25] Amine Laghrib, Abdelghani Ghazdali, Abdelilah Hakim, and Said Raghay. A multi-frame super-resolution using diffusion registration and a nonlocal variational image restoration. *Computers & Mathematics with Applications*, 72(9):2535–2548, 2016. doi:10.1016/j.camwa.2016.09.013.

[26] Amine Laghrib, Aissam Hadri, Abdelilah Hakim, and Said Raghay. A new multiframe super-resolution based on nonlinear registration and a spatially weighted regularization. *Information Sciences*, 493:34–56, 2019. doi:10.1016/j.ins.2019.04.029.

[27] Amine Laghrib, Aissam Hadri, Moad Hakim, and Hssaine Oummi. An improved PDE-constrained optimization fluid registration for image multi-frame super resolution. *RAIRO-Operations Research*, 56(4):3047–3069, 2022. doi:10.1051/ro/2022137.

[28] Baraka Jacob Maiseli, Nassor Ally, and Huijun Gao. A noise-suppressing and edge-preserving multiframe super-resolution image reconstruction

method. *Signal Processing: Image Communication*, 34:1–13, 2015. doi:10.1016/j.image.2015.03.001.

[29] Mourad Nachaoui, L Afraites, and Amine Laghrib. A regularization by denoising super-resolution method based on genetic algorithms. *Signal Processing: Image Communication*, 99:116505, 2021. doi:10.1016/j.image.2021.116505.

[30] Mourad Nachaoui and Amine Laghrib. An improved bilevel optimization approach for image super-resolution based on a fractional diffusion tensor. *Journal of the Franklin Institute*, 359(13):7165–7195, 2022. doi:10.1016/j.jfranklin.2022.07.016.

[31] Stanley J. Osher, Martin Burger, Donald Goldfarb, Jinjun Xu, and Wotao Yin. An iterative regularization method for total variation-based image restoration. *Multiscale Modeling & Simulation*, 4(2):460–489, 2005. doi:10.1137/040605412.

[32] Konstantinos Papafitsoros and Carola-Bibiane Schönlieb. A combined first and second order variational approach for image reconstruction. *Journal of Mathematical Imaging and Vision*, 48(2):308–338, 2014. doi:10.1007/s10851-013-0445-4.

[33] Matan Protter, Michael Elad, Hiroyuki Takeda, and Peyman Milanfar. Generalizing the nonlocal-means to super-resolution reconstruction. *IEEE Transactions on Image Processing*, 18(1):36–51, 2008. doi:10.1109/TIP.2008.2008067.

[34] Diego A. Sorrentino and Andreas Antoniou. Storage-efficient quasi-Newton algorithms for image super-resolution. In *16th International Conference on Digital Signal Processing, DSP 2009*, pages 1–6. IEEE, 2009. doi:10.1109/ICDSP.2009.5201145.

[35] Heng Su, Nan Jiang, Ying Wu, and Jie Zhou. Single image super-resolution based on space structure learning. *Pattern Recognition Letters*, 34(16):2094–2101, 2013. doi:10.1016/j.patrec.2013.07.012.

[36] Kaicong Sun and Sven Simon. Bilateral spectrum weighted total variation for noisy-image super-resolution and image denoising. *IEEE Transactions on Signal Processing*, 69:6329–6341, 2021. doi:10.1109/TSP.2021.3127679.

[37] Tuomo Valkonen, Kristian Bredies, and Florian Knoll. Total generalized variation in diffusion tensor imaging. *SIAM Journal on Imaging Sciences*, 6(1):487–525, 2013. doi:10.1137/120867172.

[38] Shuyuan Yang, Min Wang, Yaxin Sun, Fenghua Sun, and Licheng Jiao. Compressive sampling based single-image super-resolution reconstruction by dual-sparsity and non-local similarity regularizer. *Pattern Recognition Letters*, 33(9):1049–1059, 2012. doi:10.1016/j.patrec.2012.02.006.

[39] Xianfeng Yang and Jian Yang. Efficient diffeomorphic metric image registration via stationary velocity. *Journal of Computational Science*, 30:90–97, 2019. doi:10.1016/j.jocs.2018.11.011.

[40] Y-L You and Mostafa Kaveh. Fourth-order partial differential equations for noise removal. *IEEE Transactions on Image Processing*, 9(10):1723–1730, 2000. doi:10.1109/83.869184.

[41] Qiangqiang Yuan, Liangpei Zhang, and Huanfeng Shen. Multiframe super-resolution employing a spatially weighted total variation model. *IEEE Transactions on Circuits and Systems for Video Technology*, 22(3):379–392, 2012. doi:10.1109/TCSVT.2011.2163447.

[42] Linwei Yue, Huanfeng Shen, Jie Li, Qiangqiang Yuan, Hongyan Zhang, and Liangpei Zhang. Image super-resolution: The techniques, applications, and future. *Signal Processing*, 128:389–408, 2016. doi:10.1016/j.sigpro.2016.05.002.

[43] Kai Zhang, Wangmeng Zuo, Yunjin Chen, Deyu Meng, and Lei Zhang. Beyond a Gaussian denoiser: Residual learning of deep cnn for image denoising. *IEEE Transactions on Image Processing*, 26(7):3142–3155, 2017. doi:10.1109/TIP.2017.2662206.

[44] Wen-Yi Zhao, Harpreet S. Sawhney, Michael W. Hansen, and Supun Samarasekera. Super-fusion: A super-resolution method based on fusion. In *16th International Conference on Pattern Recognition, ICPR 2002*, pages 269–272. IEEE Computer Society, 2002. doi:10.1109/ICPR.2002.1048290.